



## NoRMCorre: An online algorithm for piecewise rigid motion correction of calcium imaging data



Eftychios A. Pnevmatikakis\*, Andrea Giovannucci

Center for Computational Biology, Flatiron Institute, Simons Foundation, New York, NY 10010, USA

### HIGHLIGHTS

- A method for non-rigid motion registration of calcium imaging data is proposed.
- The method is fast and can be run online on large volumes of streaming data.
- New metrics are proposed to quantitatively assess the registration quality.
- Implementations in Matlab and Python are provided.

### ARTICLE INFO

#### Article history:

Received 17 February 2017

Received in revised form 27 July 2017

Accepted 28 July 2017

Available online 3 August 2017

MSC:  
00-01  
99-00

Keywords:  
Calcium imaging  
Motion correction  
Image registration

### ABSTRACT

**Background:** Motion correction is a challenging pre-processing problem that arises early in the analysis pipeline of calcium imaging data sequences. The motion artifacts in two-photon microscopy recordings can be non-rigid, arising from the finite time of raster scanning and non-uniform deformations of the brain medium.

**New method:** We introduce an algorithm for fast Non-Rigid Motion Correction (NoRMCorre) based on template matching. NoRMCorre operates by splitting the field of view (FOV) into overlapping spatial patches along all directions. The patches are registered at a sub-pixel resolution for rigid translation against a regularly updated template. The estimated alignments are subsequently up-sampled to create a smooth motion field for each frame that can efficiently approximate non-rigid artifacts in a piecewise-rigid manner.

**Existing methods:** Existing approaches either do not scale well in terms of computational performance or are targeted to non-rigid artifacts arising just from the finite speed of raster scanning, and thus cannot correct for non-rigid motion observable in datasets from a large FOV.

**Results:** NoRMCorre can be run in an online mode resulting in comparable to or even faster than real time motion registration of streaming data. We evaluate its performance with simple yet intuitive metrics and compare against other non-rigid registration methods on simulated data and *in vivo* two-photon calcium imaging datasets. Open source Matlab and Python code is also made available.

**Conclusions:** The proposed method and accompanying code can be useful for solving large scale image registration problems in calcium imaging, especially in the presence of non-rigid deformations.

© 2017 The Author(s). Published by Elsevier B.V. This is an open access article under the CC BY-NC-ND license (<http://creativecommons.org/licenses/by-nc-nd/4.0/>).

### 1. Introduction

Calcium imaging methods enable monitoring large neural populations over long periods of time with single neuron resolution. Before addressing specific scientific questions, the analyst needs to pre-process the data and extract neural signals of interest from the fluorescence microscopy images/volumes. The typical

calcium imaging pre-processing pipeline consists of motion correction/image registration of the time series, followed by source extraction, where the different neurons and processes along with their neural activity time series are extracted. In this paper we focus on the motion correction pre-processing step: we introduce an algorithm for Non-Rigid Motion Correction (NoRMCorre), that is suitable for the registration of large scale planar or volumetric imaging data, and we evaluate its performance against state-of-the-art algorithms.

The general field of image registration has a long history and is still very active with many available different methods. In the con-

\* Corresponding author.

E-mail address: [epnevmatikakis@flatironinstitute.org](mailto:epnevmatikakis@flatironinstitute.org) (E.A. Pnevmatikakis).

text of calcium imaging, an algorithm needs to be (i) fast, given that each experiment typically consists of tens of thousands of frames, (ii) robust to measurement noise and neural variability/activity, and (iii) able to deal with non-rigid motion artifacts occurring from natural brain movement and/or slow raster scanning. It is generally assumed that at any point in time the brain moves uniformly. In several cases rigid translation accounts for most of the motion, and fast methods based on template alignment are often used (Thevenaz et al., 1998; Guizar-Sicairos et al., 2008; Dubbs et al., 2016). Nevertheless non-rigid artifacts can even arise from fast spatially uniform motion because of the finite time required from the microscope to scan the entire FOV. To deal with such artifacts, a common strategy is to correct each scanning line (or a contiguous group of them) separately and combine the results. Available approaches include the work of Greenberg and Kerr (2009) which is based on the Lucas-Kanade method (Lucas et al., 1981), Hidden Markov Model (HMM) approaches (Dombeck et al., 2007; Kaifosh et al., 2014), and block-wise rigid registration (Pachitariu et al., 2016).

Nevertheless, as technological advances enable the imaging of increasingly larger FOV, movements that are spatially non-uniform are likely to arise because of the finite speed at which mechanical displacements propagate through the brain, a viscoelastic medium Collman (2010). Indeed, FOV with dimensions in the order of hundreds of microns present motion patterns that cannot be explained by rigid brain deformations (Fig. 1a) or scanning artifacts. In modern experimental conditions, with animal preparations locomoting or otherwise moving under fixed or head-mountable microscopes, the mechanical strain can be significant, leading to potentially non-rigid deformations (e.g., Sekiguchi et al., 2016).

Our proposed algorithm is based on template alignment and operates by estimating a non-uniform yet smooth motion field that is then applied to each frame. Our goal is not to take a completely new approach to motion correction, but rather to present and to make available a robust alignment method that combines two important features:

- *Online processing:* NoRMCorre operates by matching patches of each given frame against a template that is continuously updated based on previously registered frames. As such, it requires access only to the current frame to be registered and the running template, plus possibly a small buffer to store past templates. Consequently it is suitable for online registration of high volume streaming data, a useful feature that can facilitate closed loop all optical interrogation experiments (Packer et al., 2015), or compensate for limited amounts of available memory.
- *Fast, non-rigid registration:* NoRMCorre splits the field of view (FOV) into overlapping patches that are registered separately and then merged by smooth interpolation. As such, it overcomes the shortcomings of rigid motion alignment without a significant computational cost, thus remaining applicable to large scale datasets. In contrast with the other available non-rigid registration methods that split the FOV only along one axis to capture the non-rigid artifacts caused by the finite speed of raster scanning, NoRMCorre can account for non-uniform artifacts along all axes, aiming to capture non-rigid brain movement as well.

We present applications to simulated and resonant scanning two-photon microscopy data and compare our method against other non-rigid image registration methods, using three custom metrics that quantify performance in terms of the crispness of registered data and estimates of residual motion. Our results indicate that NoRMCorre achieves state of the art results while operating at a speed not significantly slower than template based rigid alignment.

## 2. Materials and methods

### 2.1. Algorithm description

#### 2.1.1. Registering a frame against a given template

NoRMCorre can operate in a rigid or piecewise-rigid (pw-rigid) fashion. For rigid registration, every frame is aligned against a calculated template at a subpixel resolution using the method proposed by Guizar-Sicairos et al. (2008): the displacement vector is computed by locating the maximum of the cross-correlation between the frame and the template. The cross-correlation is efficiently obtained via fast Fourier transform (FFT) methods, and subpixel registration is achieved at a moderate computational and memory cost by upsampling the discrete Fourier transform only around the location of the identified maximum, and then refining the translation estimate. In the case of high signal-to-noise ratio (SNR), phase correlation can also be used.

Under the pw-rigid approach, the FOV in any given frame is split into a set of overlapping patches (Fig. 1b) with user determined dimensions and amount of overlap. Each patch is registered against the template, restricted to the same part of the FOV, at a subpixel resolution. Next, each patch is further split into smaller overlapping subpatches and similarly, the computed displacement vectors for the set of the initial patches are upsampled to create a smooth motion field. This associates to each subpatch a new translation vector that is subsequently rigidly applied to it (Fig. 1b). The registered subpatches are then embedded and interpolated within the original FOV to obtain the registered frame. That frame is also used to update the template in the online scenario as discussed in the following section. A block diagram of the registration pipeline is depicted in Fig. 1c.

#### 2.1.2. Updating the template

The template is updated every  $b_w$  frames (e.g.,  $b_w = 200$ ). Once  $b_w$  frames are registered against a fixed template, their average (e.g., mean or median) is computed. These averages are stored in a buffer that keeps at most the last  $b_p$  averages (e.g.,  $b_p = 50$ ). The new template is generated by averaging (e.g., by again taking the mean or median) the buffer content. Based on empirical observation, as a default choice, we compute each element of the buffer as the mean of the last  $b_w$  registered frames, and the template is generated by the median of the buffer elements. The template can be initialized by computing the median of the first few frames (or just the median of a random subset of frames). Since the template at the beginning might not be accurate, it is usually a good practice to revisit the first few frames (e.g., first  $b_w$  or  $2b_w$  frames) and register them again against a more stabilized template.

#### 2.1.3. Online vs offline

NoRMCorre is, in principle, an online and one-pass algorithm in which each frame is registered based on the current estimate of the template. However, several expedients can be used to improve its performance when the data and memory are available. For example, to avoid the influence of slow motion trends, especially at the beginning of the motion correction process, we can randomly permute the frame order prior to any registration, or start from the middle time point of the dataset and continue outwards towards the beginning/end. Moreover, when operating in offline mode, the frames within each minibatch to be registered with a fixed template can be processed in parallel, leading to potentially significant computational gains.

#### 2.1.4. Application of the shifts

Application of the computed displacement vectors (shifts) is trivial when the shifts are integer, since it corresponds to simple row/column shifting and no interpolation is required. For frac-

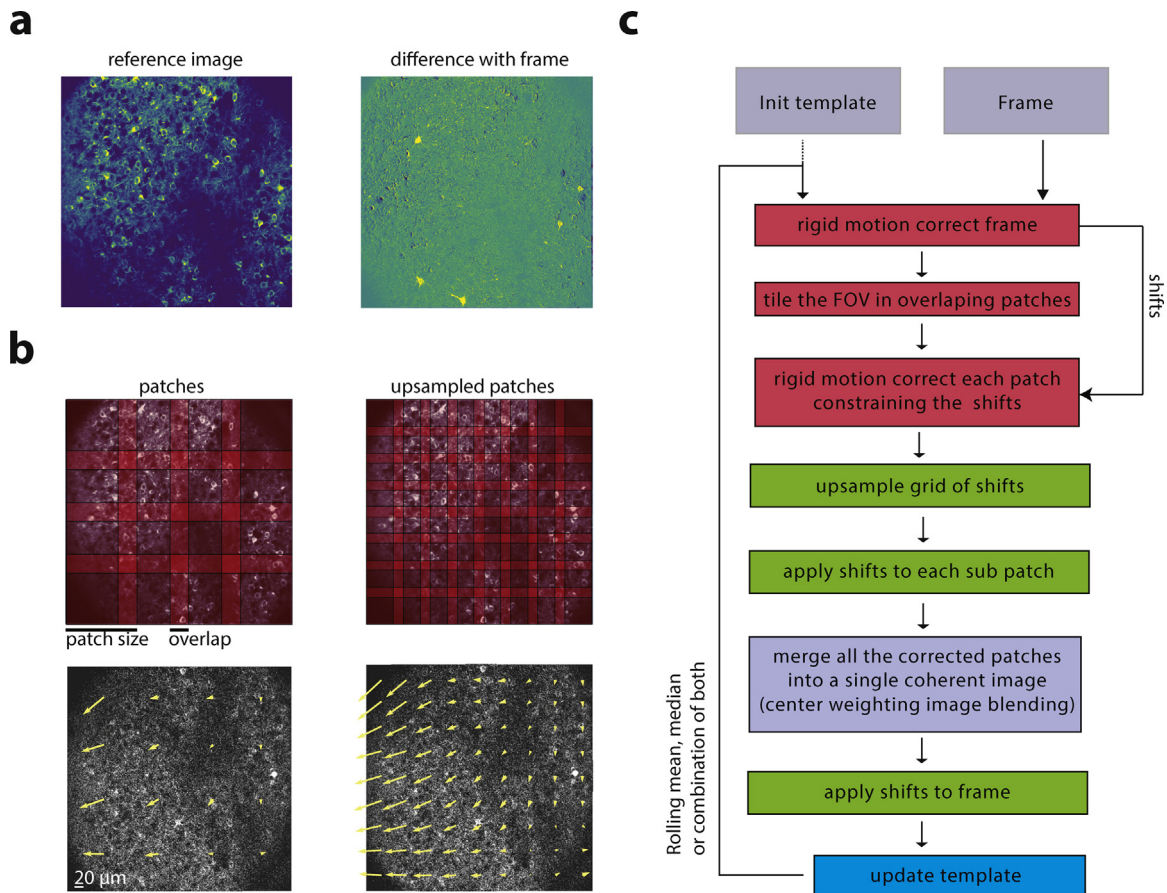


**Fig. 1.** Schematic representation of problem and proposed algorithm. *a*: Effect of non-rigid motion on frames. *Left*: A reference frame obtained by averaging across time the movie. Neurons (ring shaped) appear in most locations in the FOV. *Right*: Difference between the reference image and a frame of the movie. Active neurons appear as dense bright blobs. Neurons that were displaced by tissue movement appear as rings, caused by the mutated location of the cell membranes. Several rings are visible around the borders but not in the center, demonstrating that the tissue was displaced non uniformly (more close to the borders and less in the center). *b*: Illustration of the scheme used to overlap patches and of the upsampling process for the patches (*top*), and the displacement vectors (*bottom*). The yellow arrows represent the direction and magnitude of the motion field. *c*: Pipeline for pw-rigid registration with NoRMCorre of a frame against a given template, and template updating. (For interpretation of the references to color in this legend, the reader is referred to the web version of the article.)

tional shifts multiple interpolation methods are available, based on either space (e.g., bilinear, bicubic) or frequency domain interpolation (FFT-based). The choice of interpolation method can lead to noticeably different results, a fact often overlooked. While frequency domain methods can be slower (since they require the computation of an inverse FFT), they tend to preserve more structure because they retain more frequency content of the signal and do not introduce any smoothing effects. For example, a rigid translation corresponds to a simple phase modulation in the frequency domain, which leaves invariant the power spectrum density of the image. Therefore, frequency interpolation also preserves the original SNR, as opposed to spatial interpolation methods that smooth the signal and increase the SNR. We discuss this issue in more detail in Section 3, where we show that frequency domain interpolation leads to crisper image statistics compared to spatial interpolation. Since spatial smoothing can always be achieved post-registration, by default we use frequency domain interpolation. Frequency interpolation can lead to registered data frames with values outside the dynamic range of the original data. In practice, we preserve this dynamic range by restricting the registered frame to values between the minimum and maximum of the original frame.

## 2.2. Evaluation metrics

Typically, motion correction algorithms for calcium imaging data are evaluated on artificial datasets where known shifts are

applied to registered data. On real data however, evaluation typically occurs by visual inspection, i.e., users observe the data (or a temporally downsampled version of it) before and after registration to assess the outcome of the registration. This makes the comparison of different algorithms difficult and subjective especially when applied to real datasets. Here, we use a series of simple metrics to quantify the performance of different algorithms. In Section 3 we show that such metrics can be important for identifying locations where pw-rigid motion correction improves significantly upon simple rigid registration, a strenuous task if performed manually.

### 2.2.1. Correlation with the mean (CM) metric

To evaluate the results of the motion correction algorithm across the different frames, we use a metric that is based on the similarity (pixel-wise, Pearson's correlation coefficient  $r$ ) between the mean image across time and each individual frame. Intuitively, an increase in the correlation coefficient for a given frame indicates a better alignment with the mean. Similar metrics have been used before for assessing the quality of registration algorithms in the context of fluorescence microscopy (Lee et al., 2014). To account for border effects during registration, a number of pixels around each boundary (e.g., equal to the maximum shift in each direction over time) is removed prior to computing the correlation coefficients.

The CM metric can be used to identify frames where the registration is successful or not, or to compare different motion correction

algorithms at the level of individual frames. However, this metric critically depends on the smoothness properties of each frame which, as discussed in Section 3, can be affected by the method used to apply the computed displacements. In what follows, when using this metric we compare algorithms that register frames by applying shifts with the same method.

### 2.2.2. Crispness and focus measures

An alternative measure is to quantify how crisp is a summary image before and after registration. This can be done by computing the norm of the gradient field of the image at all pixels. If  $I$  is the summary image then its crispness can be defined as

$$c(I) = \|\nabla I\|_F, \quad (1)$$

where  $\nabla I$  denotes the gradient vector field of  $I$  in all directions,  $|\cdot|$  denotes the entry-wise magnitude, and  $\|\cdot\|_F$  denotes the Frobenius norm. Examples of summary images include the mean image and the correlation image (CI).<sup>1</sup> Intuitively, a dataset with non-registered motion will have a blurred mean image, resulting in a lower value for the total gradient field norm. Other measures of focus of the summarizing image can also be used. Similarly to the CM metric, the choice of interpolation method can affect the crispness of the CI, since the introduction of smoothing in each frame gives rise to a higher valued CI with lower crispness. The effect on the crispness of the mean image is milder as the mean image is smooth due to the averaging over time (see also the results in Section 3).

### 2.2.3. Residual optical flow (ROF) quantification

To evaluate the performance of a registration algorithm, we can attempt to quantify the motion before and after registration by using a different algorithm. In Section 3, we use the dense optical flow (OF) algorithm of Farnebäck (2003) to estimate the residual optical flow (ROF) and thus quantitatively evaluate the performance of the registration. The dense OF algorithm attempts to match the current frame to the template by estimating locally smooth displacement fields. While powerful in estimating non-rigid motion fields, the dense OF is computationally expensive and can be particularly sensitive to the low/mid-SNR conditions of typical calcium imaging datasets; as such, we do not consider it as an appropriate method for registering calcium imaging data (see Section 3.1). Therefore, to quantify the ROF after applying a registration method, we apply the dense OF algorithm on a temporally downsampled version of the registered dataset. Downsampling by a factor of  $s$  occurs by computing the temporal average of  $s$  contiguous non-overlapping frames, thus increasing the SNR which ensures robustness (and enhances computational tractability).

### 2.2.4. Dependence on neural activity

The CM and ROF metrics quantify performance on each individual frame of the dataset (or a downsampled version of it). As such, they depend not only on the quality of the registration and noise level but also on the level of neural activity. In practice we find that neural activity affects these metrics only mildly and does not affect the qualitative assessment of motion correction. We discuss this issue in more detail in Section 3.3, where we present a registration example on a dataset in which recordings from both a functional and a structural channel are available.

<sup>1</sup> The correlation image value at each pixel is the average of the correlation coefficients across time between the pixel and its neighbors (Smith and Häusser, 2010).

## 2.3. Technical details

The process of splitting the FOV into patches, registering them separately, and then combining the results together entails a few technical details that are described below.

### 2.3.1. Restricting maximum shifts

In the case where the FOV is sparsely labeled or a frame is corrupted, the registration process of two neighboring patches can produce very different displacement vectors (shifts), which can lead to corrupted registered frames. To avoid such events, the shifts allowed by the algorithm are constrained within a user defined region. In practice, for each frame, NoRMCorre first computes the rigid displacement vector for the whole frame  $\mathbf{d}$ , with a user defined maximum allowed value, e.g.,  $\|\mathbf{d}\|_\infty \leq M$ , where  $M$  is the maximum allowed displacement (assumed here to be the same in each direction for ease of notation), and  $\|\cdot\|_\infty$  denotes the  $l_\infty$  (max) norm. The shift  $\mathbf{d}^i$  for each patch  $i$  is then constrained to be within  $n$  pixels of the rigid displacement vector, i.e.,  $\|\mathbf{d}^i - \mathbf{d}\|_\infty \leq n$ , along each coordinate. From the triangle inequality the shift of each patch is bounded as  $\|\mathbf{d}^i\|_\infty \leq M + n$ .

### 2.3.2. Merging overlapping patches

To apply the shifts on overlapping patches we construct a set of linear interpolating functions that are used to ensure a smooth transition between registered neighboring patches. Consider patch  $i$ , centered around the point  $(x_i, y_i)$  with size  $(s_x, s_y)$  and overlap  $(o_x, o_y)$ , resulting in a total size  $(s_x + 2o_x, s_y + 2o_y)$ . We define the trapezoid function

$$b_X^i(x) = \begin{cases} 1, & |x - x_i| \leq s_x/2 \\ \frac{s_x + 2o_x - 2|x - x_i|}{2o_x}, & s_x/2 \leq |x - x_i| \leq s_x/2 + o_x \\ 0, & |x - x_i| > s_x/2 + o_x \end{cases}, \quad (2)$$

similarly the function  $b_Y^i(\cdot)$ , and the 2d function

$$B^i(x, y) = b_X^i(x)b_Y^i(y). \quad (3)$$

If  $I^i$  is the registered  $i$ th patch of the frame,  $i = 1, \dots, K$ , extended to the whole FOV, the interpolated registered frame is then given by

$$I(x, y) = \frac{\sum_{i=1}^K I^i(x, y)B^i(x, y)}{\sum_{i=1}^K B^i(x, y)}. \quad (4)$$

### 2.3.3. Avoiding smearing by upsampling

Interpolation can introduce smearing effects when the shifts of neighboring patches differ significantly. Consider the case of two patches overlapping along the  $x$ -direction, whose  $x$ -shifts differ by exactly 1 pixel. During interpolation, the registered overlapping region will be simply a weighed average of two consecutive non-matching pixels along the  $x$ -direction, leading to a smeared result. We empirically observed that smearing occurs when shifts in overlapping patches differ by more than 0.5 pixels.

Upsampling the initial grid of overlapping patches to a finer grid of smaller overlapping patches (Fig. 1b) can alleviate this undesirable outcome. For example, if we upsample the grid by a factor of 2, the difference in the upsampled neighboring shifts will be  $\sim 0.5$  pixels, preventing smearing. Conceptually, the grid could be upsampled up to the point where each pixel has its own displacement vector. However, this approach can be computationally very expensive when frequency domain interpolation is employed. In theory, the upsampling factor can be chosen so that it fulfills the no-smearing condition of 0.5 pixel maximum difference between the shifts of two neighboring patches. If  $n$  denotes the maximum deviation from the rigid displacement for each patch, then two

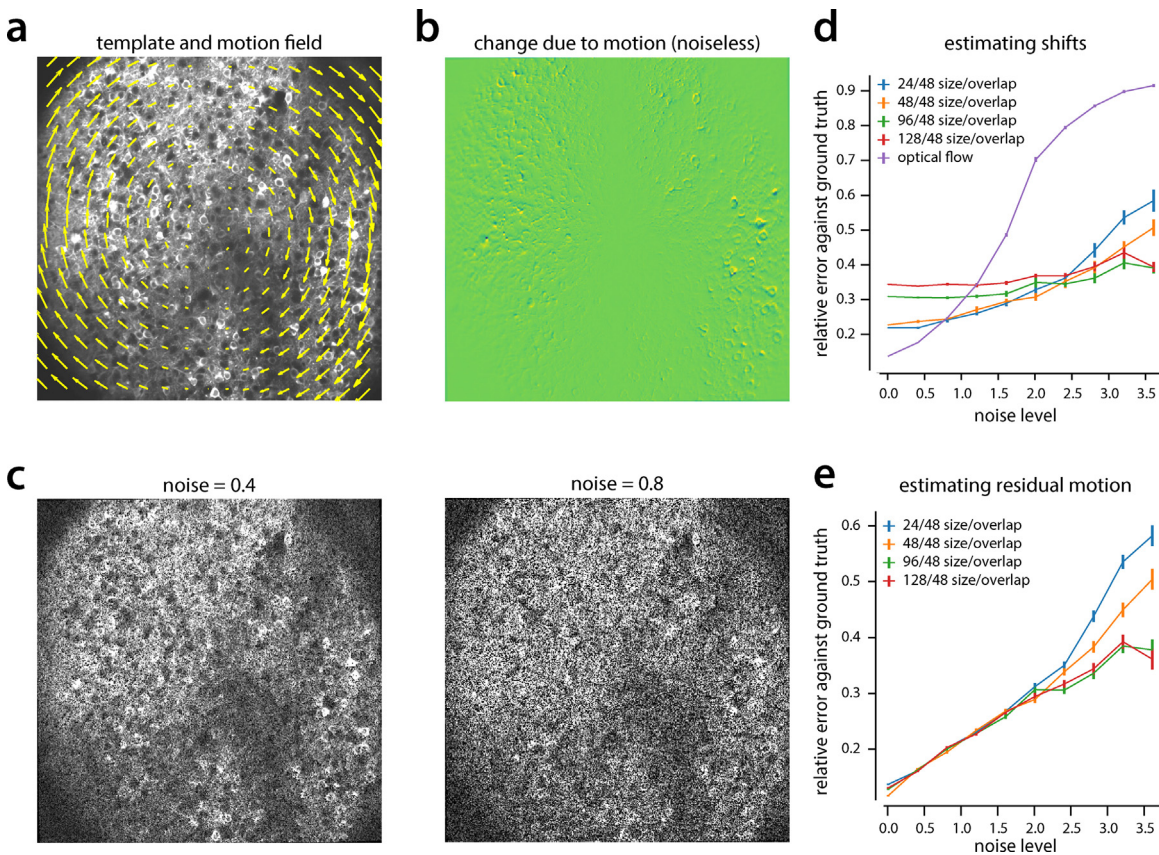


**Fig. 2.** Application of NoRMCorre to simulated data. *a*: Original image (template) and applied rotational motion field (yellow arrows). *b*: Difference between shifted noiseless image and original image. The applied transformation is non-rigid in both dimensions. *c*: Examples of noisy shifted images for two different noise levels (0.4 left, and 0.8 right, see text for details on the noise statistics). *d*: Mean relative error (ratio of the Frobenius norms of shift differences and ground truth shifts, see Appendix A.1 in supplementary material for details) between estimated shifts by NoRMCorre for different patch sizes ( $\pm$  SEM,  $n=10$ ), and estimates of dense optical flow against ground truth shifts. Smaller patches yield better approximations in high-SNR cases but are less robust for low SNR scenarios. OF is reliable only when the SNR is high. *e*: Mean relative error ( $\pm$  SEM,  $n=10$ ) between ROF and residual (difference between inferred and ground truth) shifts. Optical flow can estimate residual motion with the same fidelity for different patch sizes and is reliable for high SNR values. (For interpretation of the references to color in this legend, the reader is referred to the web version of the article.)

neighboring patches can have displacements that differ at most  $2n$  pixels in each direction (an extreme case expected to be encountered only rarely in practice), and an upsampling factor of  $4n$  guarantees the no smearing condition. In practice, for reasons of computational efficiency, we use a smaller upsampling factor, e.g., 4. For the frames where the no-smearing condition is not satisfied, merging of the overlapping patches is applied with no interpolation, i.e., the overlap size ( $o_x, o_y$ ) in Eq. (2) is set to 0.

#### 2.3.4. Choosing patch size and amount of overlap

NoRMCorre requires a template with strong reference points that facilitates robust template matching and alignment. When splitting into patches to perform pw-rigid motion correction, each patch (together with its overlap) needs to be (i) large enough to contain enough signal to produce a clear template and (ii) not too large so non-rigid motion deformations can be adequately approximated (see also Section 3.1). Empirically, for typical somatic imaging with a  $512 \times 512$  pixel FOV, an initial patch size of  $128 \times 128$  (with additional 32 pixels of overlap in each direction) is a good choice. However, if the labeling is sparse, then a larger patch size and/or overlap may be required to ensure sufficient information for robust template alignment.

#### Software

Matlab code (also applicable to 3D volumetric imaging data) is available as a standalone package at <https://github.com/simonsfoundation/NoRMCorre>. This package complements

the CNMF Matlab package for demixing and deconvolution of registered movies (Pnevmatikakis et al., 2016) available at [https://github.com/epnev/ca\\_source\\_extraction](https://github.com/epnev/ca_source_extraction). NoRMCorre is also implemented in Python at <https://github.com/simonsfoundation/CalmAn> as part of the CalmAn package (Giovannucci et al., 2017).

## 3. Results

### 3.1. Application to simulated data

We first tested NoRMCorre on simulated data with non-rigid deformation patterns. As a template we used a  $512 \times 512$  crisp noiseless image to which we applied a rotatory motion field (Fig. 2a), as an example of non-rigid deformation. The motion field was created so that every horizontal (vertical) line has average zero vertical (horizontal) movement (details are given in the supplementary material). Rigid motion correction fails since it always estimates a zero displacement vector (the overall mean), whereas existing non-rigid approaches that account for non-rigid artifacts only due to the finite raster scanning time, can approximate the displacement only along the scanning direction and estimate zero displacement in the opposite direction (data not shown). NoRMCorre was applied to the shifted image (the difference between the shifted and original image is shown in Fig. 2) plus variable amounts of noise using as template the original image. The noise model considered here was spatially uncorrelated zero mean Gaussian noise, with standard deviation for each pixel equal to the value of the pixel times a global constant  $\sigma$ . The values  $\sigma = 0.01, 0.4, 0.8, \dots, 3.6$

**Table 1**

Comparison of NoRMCorre with other non-rigid motion correction algorithm on a 2000 frame,  $512 \times 512$  pixel *in vivo* mouse cortex dataset. The average ROF values correspond to the average value per pixel for each frame (mean  $\pm$  standard deviation). The best performance according to each metric is indicated with bold.

2000 frames	Crisp (mean, a.u.)	Crisp (CI)	ROF (pixels)	Time (s)	Interp. method
Original	4301	9.87	$1.574 \pm 1.502$	—	—
Rigid	6690	10.98	$0.443 \pm 0.328$	<b>40</b>	FFT
SIMA	6678	9.25	$0.244 \pm 0.082$	530	Integer
Suite2p	6694	9	$0.246 \pm 0.08$	86	FFT
LK	6394	10.36	$0.197 \pm 0.084$	1856	Bilinear
NoRMCorre	7483	10.69	$0.154 \pm 0.09$	89	Bicubic
NoRMCorre	<b>7531</b>	<b>11.48</b>	<b><math>0.15 \pm 0.09</math></b>	117	FFT

were considered, with  $n=10$  repetitions for each noise level (see two examples in Fig. 2c).

We applied NoRMCorre with four different choices of square patch sizes (24, 48, 96, 128), always augmented with 48 pixels of overlap (24 in each side). By looking at the relative error between the estimated (upsampled to a  $512 \times 512$  resolution) and the true shifts (Fig. 2d), it is clear that NoRMCorre with small patches can better approximate smooth non-rigid deformations when the SNR is high but becomes less robust as the noise increases. On the other hand, NoRMCorre with large patch sizes ( $96 \times 96$ ,  $128 \times 128$ ) displays high robustness to noise. Fig. 2d also shows the relative error between the true motion field and the motion field estimated by the dense OF algorithm. For high SNR, the OF algorithm can estimate the motion field remarkably well, but the quality of this estimate quickly deteriorates as the noise increases, rendering dense OF inapplicable to real two-photon imaging data. We further assessed the ability of OF to quantify the performance of registration algorithms by computing the difference between the ROF as estimated on the registered images and the residual shifts, i.e., the difference between true and estimated shifts (Fig. 2e), normalized by the norm of the true shifts (see Appendix A.1 in supplementary material for a precise definition). Fig. 2e demonstrates that OF can estimate the residual motion with the same (high) fidelity, for all different patch sizes, when the SNR is high.

### 3.2. Application to *in vivo* mouse parietal cortex data

We tested the algorithm on data collected *in vivo* with a two-photon microscope on a mouse expressing GCaMP6f in the parietal cortex Koay et al. (2016), see data details in the supplementary material). The FOV had size  $512 \times 512$  pixels and the data was acquired at 30 Hz.

#### 3.2.1. Pw-rigid registration performs better than rigid registration

Fig. 3 demonstrates the performance of the rigid and pw-rigid versions of NoRMCorre on a 2000 frame segment of the dataset. According to all the considered metrics, pw-rigid motion correction led to improved registration compared to plain rigid motion correction, which in turn improved significantly over the non-registered data. Fig. 3a shows a  $100 \times 100$  pixel patch of the resulting mean for raw, rigid and pw-rigid corrected. By inspection, the pw-rigid correction preserves more fine structure, something that is also captured by the crispness of the mean metric (Table 1). The same trend is also observed for the CM metric (Fig. 3b) and the average ROF per frame metric (Fig. 3c), where the scatter plots demonstrate that the pw-rigid correction improves over the plain rigid correction for nearly all 2000 frames. Consistently, the ROF metric shows that the improvement is also global in space (every region of the FOV exhibits less movement), with most of the remaining movement estimated to be around the boundaries (Fig. 3e). Fig. 3d shows the displacements along the  $x$ -axis for a small segment of frames (black), plotted against the displacements for each of the different patches (before upsampling). Connecting with Fig. 3b, c left, we notice that pw-rigid registration improves the most over

rigid registration when the dispersion of the displacements over the different patches is high, indicating more non-uniform motion artifacts. The results are better displayed in movie format. Supplemental Movie 1 demonstrates the large variety of motion field patterns the algorithm estimates during the registration process. Supplemental Movie 2 shows a downsampled version of the results of rigid and pw-rigid registration with NoRMCorre, alongside the original data.

#### 3.2.2. NoRMCorre achieves state of the art results

Next we compared NoRMCorre in its Python implementation with (i) a Hidden Markov Model based algorithm (Dombeck et al., 2007), as implemented in the Python package SIMA (Kaifosh et al., 2014), (ii) the block-rigid approach of the Matlab package Suite2p (Pachitariu et al., 2016), and (iii) the Lucas-Kanade (LK) approach of Greenberg and Kerr (2009). These three methods are also suitable for non-rigid motion correction and have available implementations in Python (SIMA) or Matlab (Suite2p, LK). We compared the three methods with respect to the quality metrics and the speed. For reference we also include the metrics of the non-registered data as well as the performance of rigid motion correction from the Python implementation of NoRMCorre. The results (Table 1) indicate that NoRMCorre achieves the best performance for crispness metrics and residual motion at a speed comparable to rigid motion correction, which is unsurprisingly the fastest method but produces the worst results in terms of residual motion. ROF was computed with an OpenCV (v3.2, <http://opencv.org>) implementation, after  $5\times$  temporal downampling of the data to increase the SNR (see Section 2.2.3). We note that for all the other three different methods, the best and reported results were obtained by splitting the FOV into blocks tiled along the  $x$ -direction which is parallel to the raster scanning direction, demonstrating the fact that the largest part of the non-rigid artifacts may not be due to finite raster scanning time. Details of the various implementations are given in the supplementary material.

#### 3.2.3. Frequency interpolation preserves more structure of the original signal

Table 1 also illustrates the effect of the interpolation method. When applying NoRMCorre with bicubic interpolation it achieves similar residual motion compared to NoRMCorre with Fourier interpolation albeit at a higher speed. However, the crispness of the mean and mainly of the correlation image decreases due to the smoothness introduced by the bicubic interpolation. This point is highlighted even further in Fig. S1, where the correlation and mean images are shown for NoRMCorre with bicubic and FFT shifts, and the LK method that uses bilinear shifts, emphasizing the effect of different interpolation methods. Bilinear and bicubic interpolation smooths the data (Fig. S1a, left and middle), and biases upwards the correlation between neighboring pixels, as opposed to Fourier interpolation that retains the structure displayed by the weak correlations between neighboring pixels (Fig. S1a, right). On the other hand, the effect on the CM metric is opposite leading to higher values for bilinear interpolation with Lucas-Kanade regis-

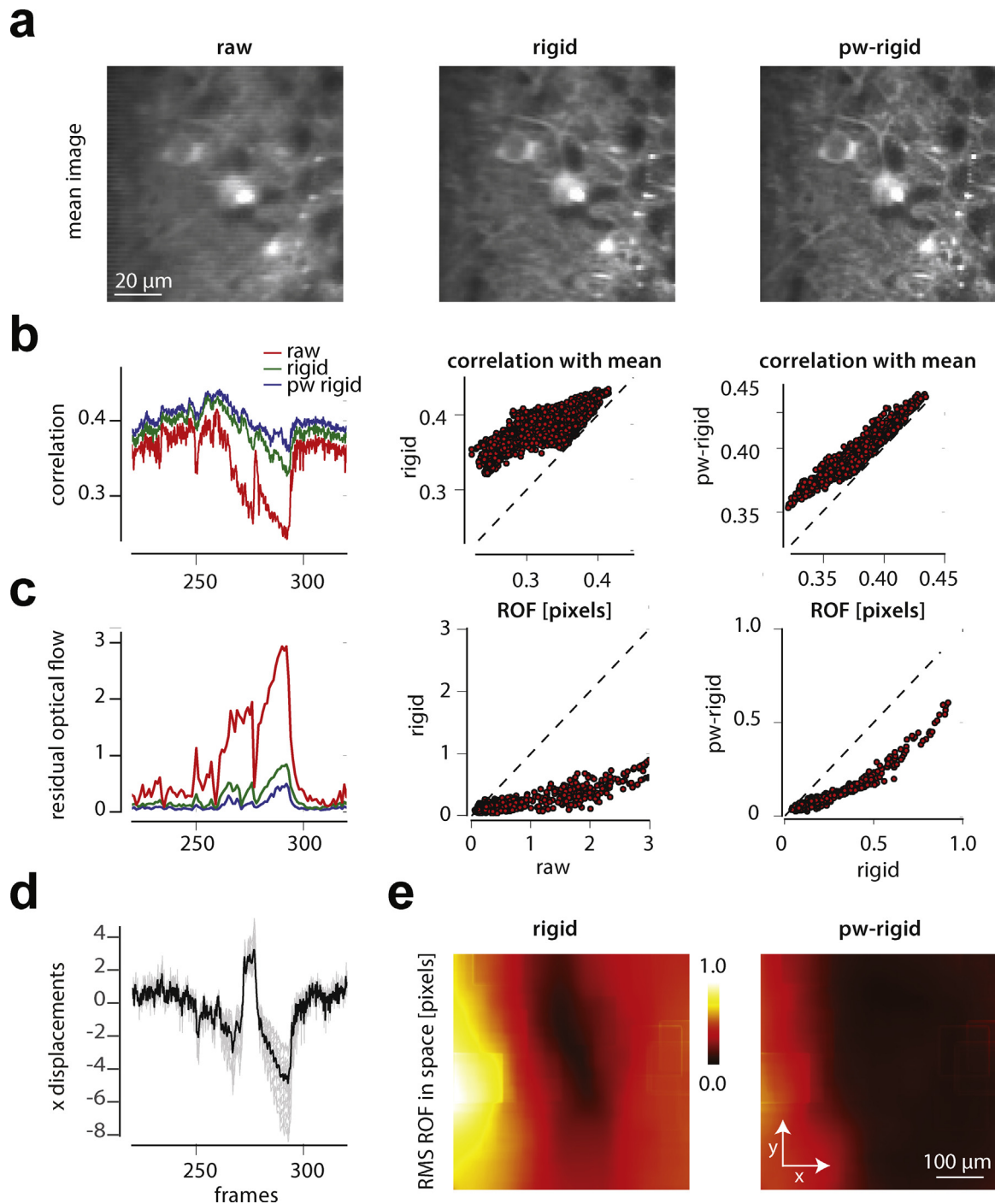


**Fig. 3.** Illustration of performance on *in vivo* mouse parietal cortex data. *a*: Mean image of raw data (focused on a  $100 \times 100$  pixel part of the FOV for clarity). Raw data (*left*), rigid corrected (*middle*) and piecewise-rigid corrected (*right*). NoRMCorre with pw-rigid correction results in a more structured mean image as quantified by the crispness of the image (*1*) ( $c(\text{raw}) = 4.3 \times 10^3$ ,  $c(\text{rigid}) = 6.69 \times 10^3$ ,  $c(\text{piecewise}) = 7.53 \times 10^3$ , measurements in absolute units). *b*: Quantification of performance based on the correlation with mean (CM) metric. For nearly every frame rigid correction improves over the raw data, and pw-rigid improves over rigid. *Left*: CM metric for a subset of frames. Scatter plot of frame-by-frame CM of raw vs rigid (*center*) and rigid vs pw-rigid (*right*). *c*, *e*: Quantification of performance using the ROF measure averaged over space (*c*, value in pixels) and over time (*e*, mean over time value of ROF in pixels). Consistently, pw-rigid correction improves over plain rigid correction (*left*, on all frames; *center*, scatter raw vs rigid; *right*, scatter rigid vs pw-rigid) and most of the remaining motion is concentrated on the boundaries of the FOV (*e*, *left*). *d*: Comparison of the rigid displacement (black) along the x-axis with the displacement of each patch for a subset of frames as computed with NoRMCorre. The main benefits from pw-rigid correction, as also can be seen from *b*, *c* (*left*), occur at frames where the displacements exhibit maximum dispersion.

tration ( $0.499 \pm 0.033$ ), and bicubic interpolation with NoRMCorre registration ( $0.443 \pm 0.017$ ), as opposed to Fourier based interpolation with NoRMCorre which achieves a significantly lower value ( $0.399 \pm 0.014$ ). This highlights the sensitivity of the CM metric on the interpolation method, and why it should be used carefully in comparisons.

### 3.2.4. Correction for motion artifacts leads to better source extraction

The main objective for correcting motion artifacts in calcium imaging data is to facilitate the downstream analysis which consists of identifying the imaged neurons and processes in the FOV and extracting their activity. Most of the algorithms used in prac-

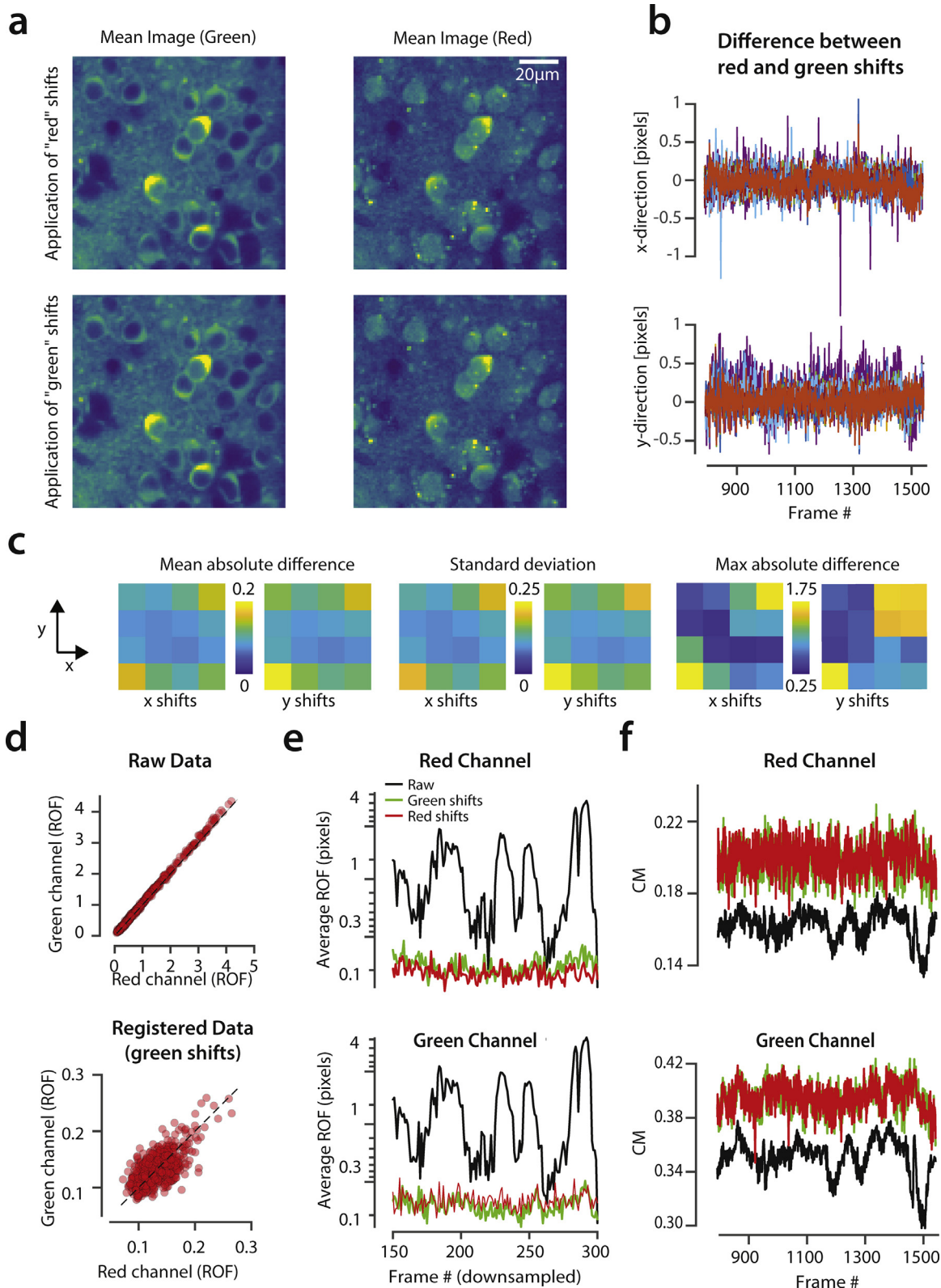


**Fig. 4.** Comparing a functional and a structural channel for motion correction: *a*: Mean images for the registered data of the functional (green) channel (*left*), and the structural (red) channel (*right*), when the displacement vectors were calculated on the red channel (*top*), and the green channel (*bottom*). All images are restricted to a  $100 \times 100$  pixel part of the FOV for clarity. In all cases, application of either the functional or the structural shifts leads to almost identical results. *b*: Differences between red and green shifts for all 16 patches along the x- (*top*) and y- (*bottom*) directions. The differences almost always remain within a very narrow range with rare exceptions. *c*: Summary statistics of the difference between red and green shifts presented in colormap form. The mean absolute difference (*left two panels*) and standard deviation (*middle two panels*) are very small, and can be below 0.1 pixels in the center of the FOV, with slightly higher values in the boundaries. The maximum difference (*right two panels*) also remains very small. *d-top*: Scatter plot of the average-per-frame ROF on the red channel vs the green channel for the raw non-registered data ( $5 \times$  downsampled). *d-bottom*: Same scatter plot this time for pw-rigidly registered data using the green shifts. In both cases, the ROF between the two channels is highly similar and very correlated, indicating that the dense OF algorithm is a reliable measure of residual motion. *e*: Average per frame ROF for raw and corrected data of red channel (*top*) and green channel (*bottom*).

**Table 2**

Comparison of registration quality of NoRMCorre using a structural vs a functional channel. Registration with either the functional or the structural channel leads to largely the same results for all metrics. The best performance according to each metric is indicated with bold.

3000 frames	Crisp (mean)	Crisp (CI)	ROF (pixels)	Correlation with mean
Original (red)	469	4.89	$0.95 \pm 0.82$	$0.161 \pm 0.008$
Rigid (red channel, red shifts)	738	9.14	$0.15 \pm 0.05$	$0.196 \pm 0.013$
Rigid (red channel, green shifts)	736	9.13	$0.15 \pm 0.05$	$0.196 \pm 0.013$
NoRMCorre (red channel, red shifts)	<b>774</b>	<b>9.17</b>	<b><math>0.1 \pm 0.02</math></b>	<b><math>0.198 \pm 0.009</math></b>
NoRMCorre (red channel, green shifts)	763	9.16	$0.12 \pm 0.03$	<b><math>0.198 \pm 0.009</math></b>
Original (green)	5926	9.49	$0.99 \pm 0.86$	$0.346 \pm 0.012$
Rigid (green channel, red shifts)	8566	11.31	$0.16 \pm 0.05$	$0.389 \pm 0.013$
Rigid (green channel, green shifts)	8622	11.38	$0.16 \pm 0.06$	$0.390 \pm 0.013$
NoRMCorre (green channel, red shifts)	8685	11.51	$0.12 \pm 0.02$	$0.391 \pm 0.011$
NoRMCorre (green channel, green shifts)	<b>8877</b>	<b>11.71</b>	<b><math>0.11 \pm 0.02</math></b>	<b><math>0.392 \pm 0.012</math></b>

tice for source extraction operate on registered data and under the assumption that each neuron retains its position in the FOV throughout the experiment. To examine the effect of registration quality we applied the CNMF source extraction algorithm (Pnevmatikakis et al., 2016) to the raw, rigidly, and registered with NoRMCorre version of the dataset, using in all cases the same parameters for the CNMF algorithm. The results (Fig. S2) indicate that the raw or rigidly registered datasets can lead to active neurons not being detected, and detected neurons being split with wrong activity traces. In contrast, the quality of the inferred sources and their activity when NoRMCorre is used is significantly higher.

### 3.3. Application to in vivo data with available structural channel recording

Dual channel recordings with a structural (red) fluorophore channel in addition to the (green) functional indicator channel are becoming ubiquitous. In principle, the structural fluorophore is static and neural activity independent, and therefore can be used to compute the displacement vectors of the dataset, which can then be applied to the functional channel. In practice this approach can be limited by a number of factors: first, structural channels can have poorer SNR compared to the functional channel. Moreover, the structural channel may not be completely static due to “leakage” from the functional channel. Finally, expression in the structural channel may be sparser (e.g., only inhibitory neurons), impeding the ability for high quality registration.

To test this approach we applied our algorithm on a different mouse *in vivo*, parietal cortex, two-photon dataset that co-expressed GCaMP6f and mCherry. The FOV was originally split in  $4 \times 4$  grid of patches each of size  $128 \times 128$  pixels with additional 32 pixels of overlap in each direction, further upsampled by a factor of 4. NoRMCorre was applied to each channel separately to estimate two sets of displacement vectors (one for the structural channel and one for the functional channel) and then each set of displacements was applied to both channels so the different registration results can be compared. A summary of this comparison can be found in Fig. 4 and Table 2. From Table 2 we see that, as before, applying non-rigid motion correction with NoRMCorre leads to better results, compared to rigid motion correction for all channels and all metrics. However, using the shifts computed in the structural (red) channel to correct the functional (green) channel does not necessarily lead to better results, with the results being perceptually identical (Fig. 4a). In fact all the metrics indicate that applying either the red or the green shifts to the data

from the same channel leads to largely similar results (Fig. 4d, e).

A more direct comparison can be made by comparing the shifts during pw-rigid registration across all patches (Fig. 4b and c). Fig. 4b shows the difference in the inferred shifts from the red and green channels for all 16 corresponding pairs of patches in both directions for a sub-interval of the recording. The difference stays very small for the majority of the frames with rare super-pixel disagreements occurring for patches in the corner of the FOV where the signal is weaker. Fig. 4c displays for all 16 pairs the mean absolute difference (left), standard deviation of the difference (middle), and maximum absolute difference (right) for both directions in colormap form. Fig. 4c demonstrates the high similarity of the inferred shifts between the two different channels, especially in the central parts of the FOV where the mean absolute, and standard deviations can be less than 0.1 pixels. For reference, when rigid motion correction was applied, the difference statistics between the shifts in the x and y directions respectively were: mean absolute difference = (0.054, 0.06), standard deviation = (0.068, 0.078) and maximum absolute difference = (0.24, 0.58) pixels. The high degree of similarity between the “red” and “green” shifts demonstrates the robustness of NoRMCorre to frame variability due to neural activity (functional indicator), as well as robustness to the type of indicator expression (cytoplasmic vs. nuclear).

The results as summarized in Table 2 and Fig. 4 also indicate the suitability of the ROF as a qualitative metric for quantifying the performance of the registration process and comparing the results of different approaches. When taken at the original data, the average OF per frame is similar for the structural ( $0.953 \pm 0.832$  pixel) vs. the functional channel ( $0.986 \pm 0.861$ ) pixel (see also Fig. 4c for a scatter plot), indicating that the optical flow estimates a very similar amount of motion for each channel, even though the two different channels record very different movies (but with the same motion). The same argument carries on for the average ROF when both channels (structural, functional) are registered with the same shifts computed from one of the two channels (Fig. 4c-bottom). A close inspection of Table 2 suggests that for a given set of shifts, the structural channel tends to have slightly lower ROF than the functional channel, which may be attributed to the functional channel’s dependence on the neural activity.

### 3.4. Application to *in vivo* mouse hippocampal data

As a final example, we applied NoRMCorre to a two-photon *in vivo* mouse hippocampal dataset of 1000 frames taken at 30 Hz (Gauthier and Tank (2016)), and compared it with other non-rigid

Results are shown for correction using both the shifts calculated on the structural channel (red) and the shifts calculated on the functional channel (green). In both cases registration using the shifts of either channel leads to very similar results (see also Table 2). f: Correlation with mean metric for raw and corrected data of red channel (top) and green channel (bottom). Again, the results indicate that correction with either channel leads to very similar results for this dataset. (For interpretation of the references to color in this legend, the reader is referred to the web version of the article.)

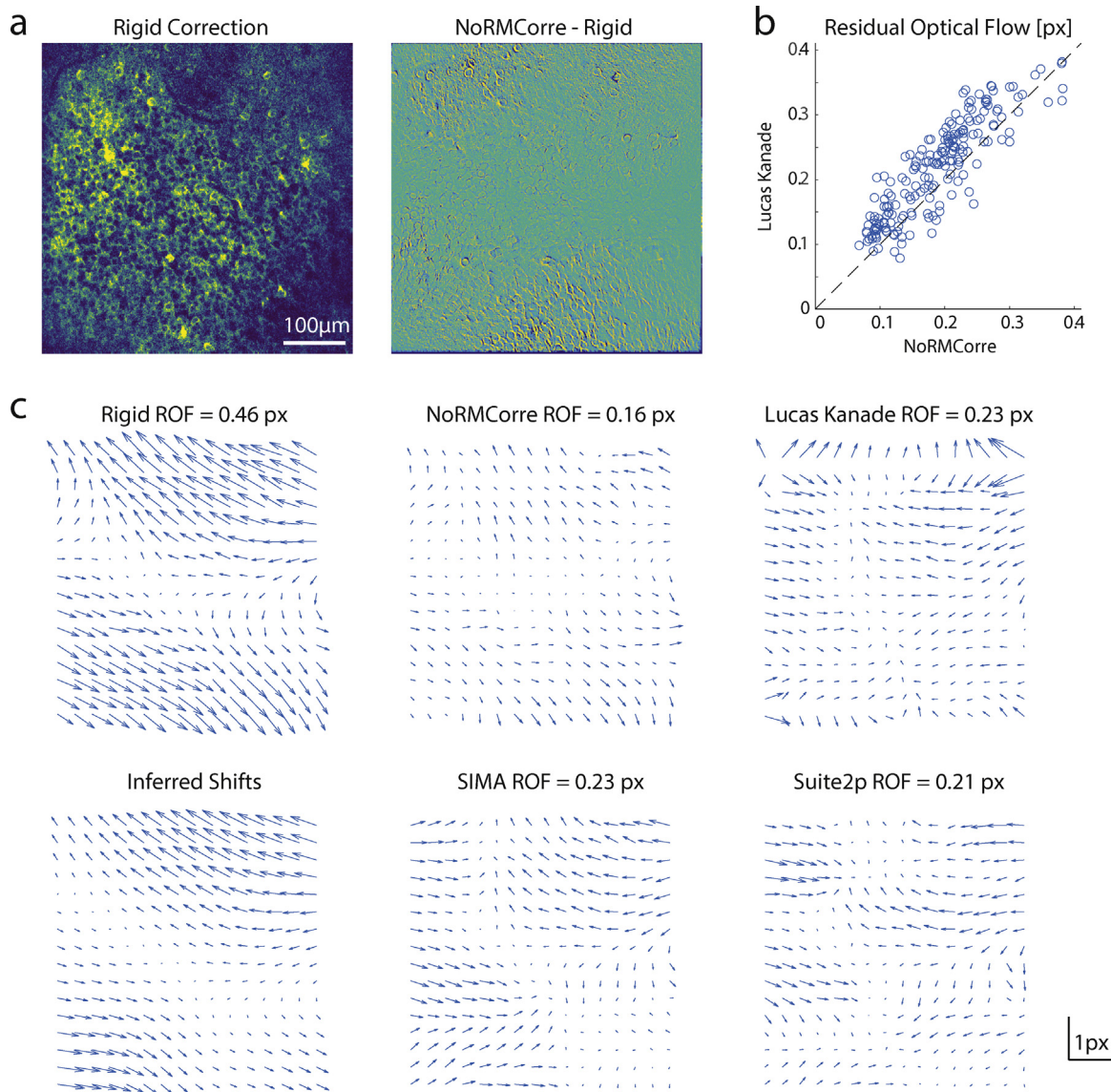


**Fig. 5.** Application to mouse *in vivo* hippocampal data and comparison with different methods. *a*: Mean of registered frames 126–130 across time for rigid registration (left) and difference of means between pw-rigid and rigid registration over all 1000 frames NoRMCorre (right). Inspection of the difference indicates non-uniform disparity between the two mean images. *b*: ROF per frame for NoRMCorre vs the LK method which was the second best performing method for this dataset. NoRMCorre outperforms LK for the majority of the frames (see also Table 3). *c*: ROF for the mean of registered frames 126–130 across time, for the 5 different methods (rigid, NoRMCorre, LK, Suite2p, and SIMA) and inferred shifts with NoRMCorre during the registration process. The inferred shifts (bottom-left) resemble closely the estimated ROF after rigid registration (top-middle), resulting in a registered frame with low ROF 0.16 pixel on average (top-right), indicating both the suitability of NoRMCorre for correcting for non-rigid distortions and the appropriateness of the ROF as a metric for assessing the registration quality.

**Table 3**

Comparison of NoRMCorre with other non-rigid motion correction algorithm on a 1000 frame, 483 × 492 pixel *in vivo* mouse hippocampal dataset. The best performance according to each metric as indicated with bold.

1000 frames	Crisp (mean)	Crisp (CI)	ROF (pixels)
Rigid	2026	15.4	$0.47 \pm 0.23$
SIMA	2090	15.1	$0.24 \pm 0.08$
Suite2p	2088	15.2	$0.24 \pm 0.09$
LK	2023	14.8	$0.23 \pm 0.09$
NoRMCorre	<b>2140</b>	<b>16</b>	<b><math>0.19 \pm 0.07</math></b>

registration methods. In this case, non-rigid registration was performed after the dataset was first registered for rigid translations. The results are summarized in Table 3 where NoRMCorre outperforms the other methods on all the proposed metrics (details of the comparison are given in the supplementary material).

Fig. 5 offers a more detailed view. Inspection of the difference between the mean images for rigidly and pw-rigidly corrected data with NoRMCorre shows non-uniform differences between the two mean images (Fig. 5a, right). NoRMCorre outperformed the LK method (which delivered the second best results) on most frames on the residual optical flow metric (Fig. 5b). Fig. 5c shows the ROF for all the different methods on the same scale computed on the mean across time of the registered frames 126–130, and the inferred shifts (Fig. 5c, bottom-left) when NoRMCorre is applied to the mean of these 5 frames. It can be seen that the inferred shifts resemble closely the measured ROF on the data before non-rigid registration (Fig. 5c, top-left) indicating that pw-rigid registration with NoRMCorre can approximate deformations that are non-rigid along both directions and cannot be attributed to just the finite scanning time. Supplementary Movie 3 displays the shifts along all 1000 frames, where it can be seen that NoRMCorre identifies and

corrects for a large variety of non-rigid transformations reminiscent of shearing and local rotations. Supplementary Movie 4 shows a sequence of non-contiguous frames taken from the temporally downsampled data from the rigidly corrected data, corrected with the LK method, and NoRMCorre, looped several times to visually enhance the non-uniform motion patterns captured and corrected by our algorithm.

#### 4. Discussion

Non-rigid artifacts within a frame can occur not only due to temporally varying motion during a period of raster scanning, but also due to elastic brain deformation within the FOV. While fast raster scanning can result in higher imaging rates for a given FOV and thus reduce the amount of intra frame motion, modern methods enable imaging of even larger areas and/or volumes (e.g., Sofroniew et al., 2016; Stirman et al., 2016) within which non-uniform motion is still possible (Collman, 2010). NoRMCorre is a simple and online method based on piecewise rigid template alignment that achieves state of the art results at a speed comparable to real time.

The pw-rigid approach used by NoRMCorre to register an individual frame is conceptually similar to the approach used in the Suite2p package (Pachitariu et al., 2016), where the FOV is split into blocks tiled perpendicularly to the scanning direction that are registered for rigid motion and then pieced together using interpolation. Similar splitting strategies are also used by the other non-rigid registration methods examined here, LK (Greenberg and Kerr, 2009) and SIMA (Kaifosh et al., 2014). However, as demonstrated through the examples presented in this paper, non-rigid motion can occur in all directions, and therefore accounting for it only in one dimension can lead to poorer registration results. Moreover, by further upsampling the patches and creating a smooth motion field NoRMCorre prevents smearing effects occurring from the registration of low SNR, sparse, or corrupted frames.

To better quantify the benefits of piecewise rigid registration over rigid registration as well as to compare NoRMCorre with other non-rigid motion registration algorithms we developed some intuitive metrics that measure the crispness of the registered images and also used independent algorithms to estimate the amount of residual motion after registration. These metrics also highlighted the importance of the interpolation method used to apply the computed displacement vectors. While the effect of the smoothing introduced by the spatial interpolation methods might be minimal, and actually create the perception of a higher SNR, we believe that the statistics of the registered data should reflect the original input as much as possible, and spatial smoothing can occur downstream in the analysis if necessary. We argued that by using the computationally more expensive Fourier based interpolation and avoiding any smoothing, one can better preserve the statistics of the originally acquired data.

The ultimate goal of motion registration is to stabilize the FOV. As explained with an example, this is important for segmentation reasons because several current source extraction methods identify sources by searching for groups of pixels that behave similarly with each other across time (Pnevmatikakis et al., 2016). An alternative to such approaches would be to track individual neurons over time, an approach that has been taken when imaging freely moving *Caenorhabditis elegans* (Nguyen et al., 2016), where the deformations can be very dramatic. However, these methods tend to be computationally very expensive and have not yet found applications in registering other types of data.

The datasets used as examples in this paper pertain to two-photon, two-dimensional, raster scanning imaging of mostly cell bodies. However, our approach can also be applied to other types of imaging datasets. For the case of one-photon, microendoscopic

data, high pass spatial filtering can be used to remove the bulk of the smooth background signal created by the large integration volume, and create stark reference points, prior to applying registration. NoRMCorre can also be readily applied to dense volumetric data (e.g., SCAPE microscopy (Bouchard et al., 2015)), where non-rigid motion can exist in all 3 directions. More details about such applications will be presented in the future.

#### Acknowledgements

We thank D. Chklovskii, J. Magland, A. Barnett (Flatiron Institute, Simons Foundation), J. Gauthier, S.A. Koay, S. Thibierge (Princeton University), F. Collman (Allen Intitute), J. Taxidis (UCLA) and N. Sofroniew (Janelia Research Campus) for useful discussions. We thank S.A. Koay, J. Gauthier and D. Tank (Princeton University) for providing us with the *in vivo* mouse cortex datasets.

#### Appendix A. Supplementary data

Supplementary data associated with this article can be found, in the online version, at <http://dx.doi.org/10.1016/j.jneumeth.2017.07.031>.

#### References

- Bouchard, M.B., Voleti, V., Mendes, C.S., Lacefield, C., Grueber, W.B., Mann, R.S., Bruno, R.M., Hillman, E.M., 2015. *Swept confocally-aligned planar excitation (scape) microscopy for high-speed volumetric imaging of behaving organisms*. *Nat. Photon.* 9, 113–119.
- Collman, F.C., 2010. *High Resolution Imaging in Awake Behaving Mice: Motion Correction and Virtual Reality*. Princeton University.
- Dombeck, D.A., Khabbaz, A.N., Collman, F., Adelman, T.L., Tank, D.W., 2007. *Imaging large-scale neural activity with cellular resolution in awake, mobile mice*. *Neuron* 56, 43–57.
- Dubbs, A., Guevara, J., Yuste, R., 2016. *moco: fast motion correction for calcium imaging*. *Front. Neuroinform.* 10.
- Farnebäck, G., 2003. *Two-frame motion estimation based on polynomial expansion*. In: Scandinavian Conference on Image analysis. Springer, pp. 363–370.
- Gauthier, J., Tank, D., 2016. *A subset of CA1 and subiculum neurons selectively encode rewarded locations*. In: Computational and Systems Neuroscience Meeting. Cosyne.
- Giovannucci, A., Friedrich, J., Deverett, B., Staneva, V., Chklovskii, D., Pnevmatikakis, E., 2017. *Caiman: an open source toolbox for large scale calcium imaging data analysis on standalone machines*. In: Computational and Systems Neuroscience Meeting. Cosyne.
- Greenberg, D.S., Kerr, J.N., 2009. *Automated correction of fast motion artifacts for two-photon imaging of awake animals*. *J. Neurosci. Methods* 176, 1–15.
- Guizar-Sicairos, M., Thurman, S.T., Fienup, J.R., 2008. *Efficient subpixel image registration algorithms*. *Opt. Lett.* 33, 156–158.
- Kaifosh, P., Zaremba, J.D., Danielson, N.B., Losonczy, A., 2014. *SIMA: python software for analysis of dynamic fluorescence imaging data*. *Front. Neuroinform.* 8.
- Koay, S.A., Engelhardt, B., Pinto, L., Deverett, B., Thibierge, S., Brody, C., Tank, D., 2016. *Neural Dynamics in a Mouse Navigation and Accumulation of Visual Evidence Task*. Society for Neuroscience, 739.07.
- Lee, S., Vinegoni, C., Sebas, M., Weissleder, R., 2014. *Automated motion artifact removal for intravital microscopy, without a priori information*. *Sci. Rep.* 4, 4507.
- Lucas, B.D., Kanade, T., et al., 1981. *An iterative image registration technique with an application to stereo vision*. *IJCAI* 81, 674–679.
- Nguyen, J.P., Linder, A.N., Plummer, G.S., Shaevitz, J.W., Leifer, A.M., 2016. *Automatically Tracking Neurons in a Moving and Deforming Brain*. arXiv preprint [arXiv:1610.04579](https://arxiv.org/abs/1610.04579).
- Pachitariu, M., Stringer, C., Schröder, S., Dipoppa, M., Rossi, L.F., Carandini, M., Harris, K.D., 2016. *Suite2p: Beyond 10,000 Neurons With Standard Two-Photon Microscopy*, pp. 061507 bioRxiv.
- Packer, A.M., Russell, L.E., Dalgleish, H.W., Häusser, M., 2015. *Simultaneous all-optical manipulation and recording of neural circuit activity with cellular resolution in vivo*. *Nat. Methods* 12, 140–146.
- Pnevmatikakis, E.A., Soudry, D., Gao, Y., Machado, T.A., Merel, J., Pfau, D., Reardon, T., Mu, Y., Lacefield, C., Yang, W., et al., 2016. *Simultaneous denoising, deconvolution, and demixing of calcium imaging data*. *Neuron* 89, 285–299.
- Sekiguchi, K.J., Shekhtmeyster, P., Merten, K., Arena, A., Cook, D., Hoffman, E., Ngo, A., Nimmerjahn, A., 2016. *Imaging large-scale cellular activity in spinal cord of freely behaving mice*. *Nat. Commun.* 7.

- Smith, S.L., Häusser, M., 2010. Parallel processing of visual space by neighboring neurons in mouse visual cortex. *Nat. Neurosci.* 13, 1144–1149.
- Sofroniew, N.J., Flickinger, D., King, J., Svoboda, K., 2016. A large field of view two-photon mesoscope with subcellular resolution for *in vivo* imaging. *eLife* 5, e14472.
- Stirman, J.N., Smith, I.T., Kudenov, M.W., Smith, S.L., 2016. Wide field-of-view, multi-region, two-photon imaging of neuronal activity in the mammalian brain. *Nat. Biotechnol.*
- Thevenaz, P., Ruttimann, U.E., Unser, M., 1998. A pyramid approach to subpixel registration based on intensity. *IEEE Trans. Image Process.* 7, 27–41.